crystals

MDPI

Article

Wood-Derived Graphite: A Sustainable and Cost-Effective Material for the Wide Range of Industrial Applications

Young Soon Kim [1], Md. Abu Hanif [1], Hyeonjin Song [1], Sungeun Kim [2], Yonu Cho [2], Seung-Kon Ryu [1] and Hong Gun Kim [1,*]

[1] Institute of Carbon Technology, Jeonju University, Jeonju 55069, Republic of Korea; kyscjb@jj.ac.kr (Y.S.K.); hanif21@jj.ac.kr (M.A.H.)
[2] Global Prodigy Academy, Jeonju 55069, Republic of Korea
* Correspondence: hkim@jj.ac.kr; Tel.: +82-63-220-3157

Abstract: The study explored the graphitization of wood through two distinct methods: a high-temperature approach at 2400 °C and a low-temperature technique at 1400 °C using a catalyst. The graphitization properties were assessed by conducting thermal experiments at various temperatures (1100 °C, 1400 °C, 1800 °C, 2000 °C, and 2400 °C), both with and without a catalyst. The development of graphite lattices was quantitatively analyzed using an array of techniques: X-ray diffractometer (XRD), Raman spectroscopy, high-resolution transmission electron microscopy (HR-TEM), and Fourier transform infrared spectroscopy (FTIR). The XRD analysis highlighted temperature-dependent changes in lattice parameters (d_{002}, L_a, and L_c), while Raman spectroscopy tracked alterations in the D to G peak ratio (D/G) with temperature. An increase in temperature is correlated with a rise in the number of graphene layers and the degree of graphitization. Notably, the process of graphite lattice formation varied across the experimental temperature spectrum. The use of a catalyst resulted in a reduced d_{002} spacing, signifying an enhanced degree of graphitization. Moreover, the catalyst promoted a consistent and smooth graphitization process throughout the heating stages. In contrast, graphitization without a catalyst occurred at higher temperatures, specifically between 1800 °C and 2000 °C, with the d_{002} value stabilizing around 0.338 nm. The catalyst proved instrumental in transforming the initial structure into well-ordered graphite at lower temperatures. This investigation underscores the potential and benefits of employing a catalyst to generate high-quality graphite from wood at reduced temperatures, paving the way for sustainable and economically viable applications of this material.

Keywords: graphitization; wood; catalyst; well-ordered graphite; interlayer space; microstructure

Citation: Kim, Y.S.; Hanif, M.A.; Song, H.; Kim, S.; Cho, Y.; Ryu, S.-K.; Kim, H.G. Wood-Derived Graphite: A Sustainable and Cost-Effective Material for the Wide Range of Industrial Applications. *Crystals* **2024**, *14*, 309. https://doi.org/10.3390/cryst14040309

Academic Editor: Jan Macutkevic

Received: 28 February 2024
Revised: 25 March 2024
Accepted: 26 March 2024
Published: 27 March 2024

1. Introduction

Non-renewable fossil fuels like coal and oil, have a number of drawbacks when it comes to creating a sustainable energy system. These drawbacks include exerting pressure on natural resources and contributing to global warming [1]. However, in contrast to coal, wood serves as a renewable energy source [2]. In addition, wood, plant, crop, fruit, and animal waste are examples of the various naturally occurring forms of biomass, which is a carbon-rich material. A carbon-rich residue is created when biomass is thermally processed in an inert atmosphere, breaking down the labile oxygen-rich structure. Since ancient times, biomass has been utilized as a source of carbon materials because of its abundance and ease of conversion. It is widely acknowledged that the highest treatment temperature and the structure of the precursor biomass determine the structure of the carbon material generated from biomass.

Charcoal, derived from wood, is another renewable energy form produced through thermal decomposition in the absence or controlled presence of oxygen. As a result, charcoal aligns with global efforts to promote renewable energy and reduce carbon dioxide

(CO_2) emissions. Interestingly, charcoal maintains a delicate balance: it emits CO_2 during combustion due to its wood composition; however, it also immobilizes CO_2 from the atmosphere [3]. Charcoal is a porous carbon material with numerous pores developed on its surface and inside. If the pores are developed, air can easily enter the inside, it is easy to burn, and it has good thermal power, so it is an excellent fuel; however, above all, the large surface area greatly increases the ability to absorb organic gases [4].

Several researchers have reported studies on producing graphite by heating charcoal made from wood to high temperatures. Graphite is largely divided into two types: natural graphite and artificial graphite. Natural graphite is obtained from minerals that exist in the form of graphite in nature. The carbon component of natural graphite is in a plate-like form, piled up layer by layer under high temperature and pressure for a long time [5]. Natural graphite is expensive, requires a difficult purifying procedure, and has inconsistent purity. Artificial graphite has several advantages over natural graphite, including stronger controllability over the synthesis process, a larger carbon source, and a greater level of purity [6]. Artificial graphite is made by heating raw materials to over 2500 °C [7]. There is growing interest in using high-density, low-volatile charcoal to manufacture graphite. This is due to the potential to reduce net greenhouse gas emissions from producing graphite from coal or coke. 'White' charcoal is expected to be a potential candidate for this application. Research by Park Yong-Nam and others also conducted research on producing graphite using white charcoal, which can replace coal or coke.

Graphite's exceptional qualities, including its high thermal and chemical stability and great electrical conductivity, are a result of its well-organized structure [8]. Due to its outstanding qualities, graphite is widely used in a variety of applications, including refractories [9], the manufacturing of graphene [10], supercapacitors [11], solar cells [12], fuel cells [13], cars [14], and batteries [15]. The researchers are still trying to find an easy, cost-effective technology to produce high-quality, well-ordered graphite. The traditional method of producing synthetic graphite involves heating raw materials like pitch and petroleum coke to high temperatures in order to transform amorphous carbon into a regular graphite structure [16,17]. This synthetic approach does, however, have a number of drawbacks, such as expensive expenses and stringent equipment needs. As a result, adding the catalyst during the graphitization process has been discovered and is proven to be a successful method of creating artificial graphite. The best method for turning biomass, a renewable carbon precursor, into graphitic carbon compounds at comparatively lower temperatures (900–1500 °C) is catalytic graphitization. Typically, this process turns amorphous carbon into ordered carbon structures, requiring a process involving a transition metal catalyst including chromium (Cr) or manganese (Mn) [18], cobalt (Co) [19], nickel (Ni) [20], etc. Because of the catalytic properties of the metal particles that develop during the procedure, some metals can lower the graphitization temperature [21].

Recently, iron-based materials are supposed to be the most widely used metal catalysts in the manner of catalytic graphitization, which produces graphitic carbon [22]. Because iron sources exist in diverse phases, the iron loading process has grown to be essential in catalytic graphitization. However, it reduces mechanical characteristics and contaminants in a furnace throughout the carbonization process. Also, this procedure employing an organic solution is mostly employed to enhance the interfacial contacts for the implantation method [23]. Thus, it is desirable to prepare for nanoparticle agglomeration and to develop a new graphitic surface modification that does not require an organic solution. Conversely, mechanically mixed approaches, such as ball milling methods, demonstrate a straightforward, quick, affordable, and environmentally friendly technology with great promise [24]. However, ineffective management of the milling process can lead to viscosity accumulation, which elongates the entire procedure and lowers milling effectiveness. Gomez-Martin et al. prepared iron-catalyzed graphitic carbon materials from biomass resources using dispersed DMF carbon sources into $FeCl_3$ solution and a furnace heated to 2000 °C [25].

In this study, we compared and analyzed high-temperature graphitization and catalytic graphitization to produce high-quality artificial graphite from wood, followed by

the carbonization of white charcoal at comparatively low temperatures, in an inexpensive, easy method, and in a sustainable way. The catalytic graphitization of wood-derived charcoal can be a more efficient and cost-effective method for producing high-quality graphite compared to traditional high-temperature methods using fossil fuels. Graphite samples can be synthesized with a controllable graphitization degree and stacking sequence depending on the presence or absence of a catalyst. Here, the iron precursor was used as a catalyst to synthesize high-quality graphite at low temperatures. The structure and chemical composition of the as-prepared graphite are investigated through XRD, Raman spectroscopy, FTIR, HR-TEM, field emission scanning electron microscopy (FESEM), and energy-dispersive X-ray spectroscopy (EDS) to trace the structural evolution during the graphitization process. We overcame the shortcomings of the synthesis of highly ordered graphite with a cost-effective catalytic method instead of a high-temperature synthesis method. Our as-synthesized graphite product can be applied in various sectors, including aerospace, energy storage, batteries, etc., mainly as an anode material.

2. Materials and Methods

2.1. Materials

The experimental material, wood-based white charcoal, was obtained from a traditional kiln in Sangdong-eup, Taebaek-gun, Gangwon-do, Republic of Korea. Initially, it was broken down into smaller pieces, and then the charcoal was finely ground into a powder. This powder was subsequently sifted through a 325 mesh (<45 μm) sieve, meeting ASTM-E-11-01 standards [26]. Iron(III) nitrate nonahydrate ($Fe(NO_3)_3 \cdot 9H_2O$, 98.5%) and hydrochloric acid (HCl, 35.0~37.0%) were purchased from Samchon Chemical Co., Ltd., Seoul, Republic of Korea. Natural graphite (commercial graphite, CG) was obtained from BTR New Material Group Co., Ltd., Guangming, China.

2.2. Synthesis of Graphite

In the comparative study, two graphitization methods were evaluated: a non-catalytic method and a catalytic method. The non-catalytic approach involved heating white charcoal to 1000 °C and 1400 °C for 60 min under a nitrogen atmosphere, designated as H1000 and H1400, respectively. This was followed by degassing at 1400 °C under a high vacuum and switching to an argon atmosphere. Higher-temperature graphitization was then conducted at 1800 °C for 60 min (H1800), 2000 °C for 30 min (H2000), and 2400 °C for 10 min (H2400). For comprehensive experimental details, see the previously published paper [27].

In the catalytic method, an aqueous $Fe(NO_3)_3 \cdot 9H_2O$ solution was mixed to achieve a 4:10 mass ratio of iron ions to white charcoal, creating catalyst particles. In order to ensure uniform dispersion, the white charcoal powder was stirred for 24 h at ambient temperature. This was followed by 4 h of continuous stirring hydrothermal synthesis at 160 °C. The resulting product undergoes filtration, distilled water washing, and drying after synthesis. The graphitization process involved sequential heating in a carbonization furnace at 1000 °C (C1000), 1200 °C (C1200), and 1400 °C (C1400) for 2 h each. The graphitized white carbon powder was acid-washed using a 2 M HCl solution to remove unwanted materials. After that, it was washed several times with distilled water and finally dried at room temperature for two days.

2.3. Characterization

The X-ray diffractometer (XRD, D8 ADVANCE, A Bruker, Karlsruhe, Germany) was employed to investigate the graphite samples' crystalline structure and phase purity. Fourier transform infrared spectroscopy (FTIR, Nicolet iS5, Thermo Fisher Scientific, Waltham, MA, USA) was used to identify the functional groups present in the as-prepared materials. The crystallinity and presence of defects in the graphite layers were assessed using the Raman spectrometer (Raman, HR-800, Horiba LabRAM, Kyoto, Japan). Raman spectra were recorded with a 10% neutral density filter, a 514 nm laser, a grating resolution of 1800 lines/mm, an acquisition time of 5 s, an accumulation count of 5, and a spectral

range of 100–4000 cm^{-1}. The powder's surface structural morphology was inspected with field emission scanning electron microscopy (FE-SEM) and energy-dispersive X-ray spectroscopy (EDS) using a Hitachi SU8600 (Tokyo, Japan). The internal structure was analyzed with in-situ high-resolution transmission electron microscopy (HR-TEM, JEOL JEM-3011 HR, Tokyo, Japan).

3. Results and Discussion

3.1. Structural Properties

The XRD spectra of the H1000, C1000, H1400, and C1400 samples are shown in Figure 1. The samples without catalyst, Figure 1a,c exhibited similar characteristic peaks of graphite, along with the broad diffraction peaks at 2θ angles of 20°~26°, and 40°~45°. These broad peaks can be attributed to the disorder graphite structure of crystal planes (002) and (100), respectively. Lee et al. [17] showed that when petroleum coke raw material was manufactured by heat treatment at 1200 °C, it was disordered graphite. In addition, when Polyvinylidene chloride (PVDC) was quickly heated (1 pulse) from 1000 degrees to 3000 °C for 1 h without a catalyst by Fogg et al. [28], the turbostratic graphite was 0.5%, i.e., mostly disordered graphite was observed, which is a similar result. The samples with Fe-impregnated as a catalyst showed in graphite contained a strong peak centered 2θ angles at approximately ~26.6° (002), ~42.5° (100), ~44.4° (101), ~50.4° (102), and ~54.0° (004) with the XRD phases of hexagonal (H) phase (Figure 1b,d). In addition, the (100) peak of the rhombohedral® phase appears at ~43.4°. In the cases of producing graphite with Fe catalyst using sawdust as a raw material by Thompson et al. [22] and Nakayasu et al. [29], the results are different from those in which (002) and (100) peaks appeared prominently without rhombohedr® (R). The hexagonal phases of the (002), (100), (101), (102), and (004) planes caused the diffraction peaks at 2θ angles of 26.23°, 42.41°, 44.36°, 50.38°, and 53.97°, respectively, as shown in Figure 1e with PDF Card No. 1011060 of hexagonal graphite structure. However, the rhombohedral phases of the (002), (100), and (222) planes caused the diffraction peaks at 2θ angles of 26.61°, 43.45°, and, 54.81°, respectively, as shown in Figure 1e with PDF Card No. 1101021 of rhombohedral. This diffraction peak corresponded to the hexagonal (H) phase and (100) peak of the rhombohedral (R) phase, of graphite, and it was also observed in the XRD pattern of commercial graphite (CG), shown in Figure 1f. The presence of a catalyst (Fe) during sample preparation leads to the formation of additional crystal phases (hexagonal and rhombohedral) alongside the typical graphite structure.

The values of the structural parameters, including the interlayer distance (d_{002} and d_{100}) and the physical dimensions of the micro-crystallite (L_c, or stack height) and L_a, or width), can be determined based on these sharp and broad peaks using the following Bragg and Scherrer equations [30,31] [Equations (1)–(4)]:

$$d = \lambda/(2\sin\theta) \quad (1)$$

$$L = K\,\lambda/(\beta\cos\theta) \quad (2)$$

$$L_c = 0.89\,\lambda/(\beta\cos\theta) \quad (3)$$

$$L_a = 1.84\,\lambda/(\beta\cos\theta) \quad (4)$$

where d refers to the interlayer distance, θ indicates the Bragg angle, λ represents the wavelength of the X-rays, β denotes the full width of half maximum, and K describes the dimensionless constant (1.84 for L_a, 0.89 for L_c). Table 1 displays the computed values for the parameters associated with the structure. The crystallite size values for synthesized graphite with a catalyst are higher than those for synthesized graphite without a catalyst. The interlayer spacing (d_{002}) of graphite produced through the heating process ranges from approximately 0.384 to 0.393 nm, whereas graphite produced using a catalytic process exhibits a d_{002} value between 0.337 and 0.339 nm. This indicates that the lattice spacing is larger for the heat-treated graphite compared to the catalytically synthesized graphite. Consequently, it is evident that the use of a catalyst at the same temperature results in a

more densely packed lattice structure. Furthermore, graphite produced with a catalyst closely resembles the d_{002} lattice spacing of commercially available graphite, which is approximately 0.338 nm. However, the ratio of L_c/d_{002} is more than double, signifying a higher degree of graphitization when a catalyst is employed at the same temperature. Li et al. produced graphite by pyrolyzing five different coal types. In samples from the Xinjing Coalfield in Shanxi Province, the d_{002} was (0.348 nm), d_{100} was (0.205 nm), L_c was (2.090 nm), L_a was (1.233 nm), and the L_c/d_{002} ratio was 6.0 [32]. Furthermore, Deraman et al. heat-treated food-grade wheat starch powder at 1000 °C and found a d_{002} of (0.394 nm), d_{100} of (0.210 nm), L_c of (2.548 nm), L_a of (5.328 nm), and an L_c/d_{002} ratio of 6.5. When compared to C1000 and C1400, the L_c was about 4~5 times, and the number of stacked carbon planes (n) was also about a third [33]. In Destyorini et al.'s study using a Ni catalyst, at 1300 °C, d_{002} was (0.337 nm), L_c was (46.36 nm), and the L_c/d_{002} ratio was (137.44). This indicated that L_c was approximately 4.5 times smaller compared to C1400, which used Fe as a catalyst [34].

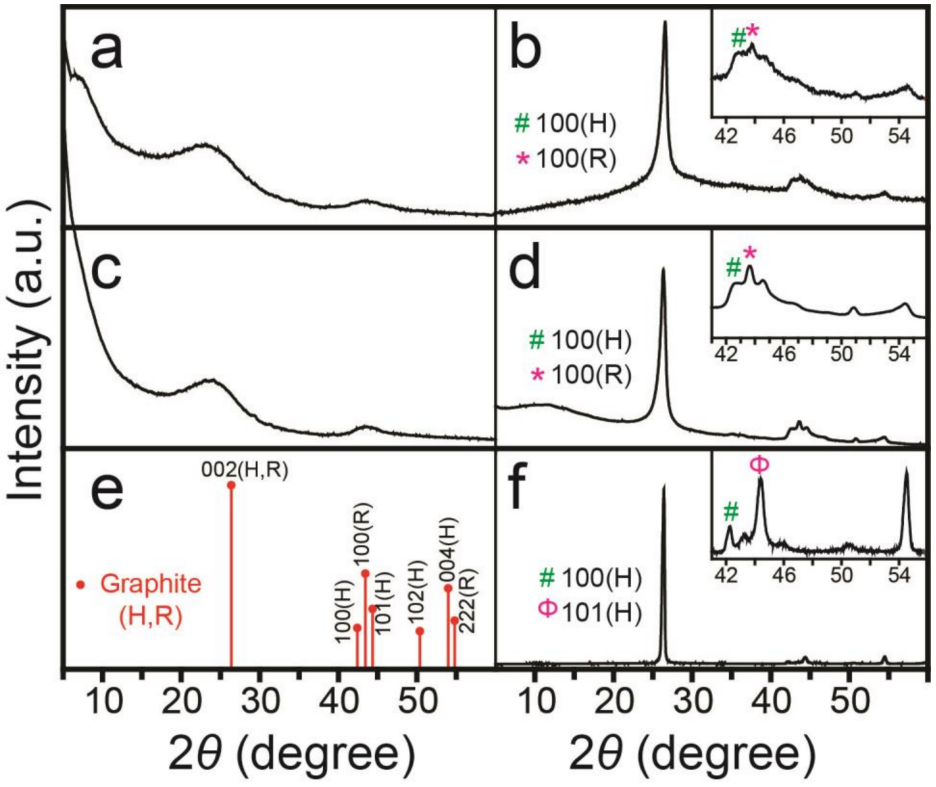

Figure 1. XRD spectra of graphite for (**a**) H1000, (**b**) C1000, (**c**) H1400, (**d**) C1400, (**e**) graphite of hexagonal (H), rhombohedral (R) phases, and (**f**) CG.

Table 1. Interlayer spacing, crystallite dimension of L_c, L_a, and L_c/d_{002} for H1000, H1400, C1000, C1400, and commercial graphite (CG).

Samples	d_{002} (nm)	d_{100} (nm)	L_c (nm)	L_a (nm)	L_c/d_{002}
H1000	0.393	0.208	0.763	2.001	1.943
H1400	0.384	0.207	0.894	2.365	2.330
C1000	0.337	0.207	8.397	3.065	24.949
C1400	0.339	0.207	9.907	3.477	29.239
Commercial graphite (CG)	0.338	0.214	22.849	25.241	64.478
[32]	0.348	0.205	2.090	1.233	6.0
[33]	0.394	0.210	2.548	5.328	6.5
[34]	0.337	-	46.36	-	137.44

Furthermore, the XRD spectra of H1800, H2000, and H2400 samples are shown in Figure 2. The samples without catalyst, exhibited similar characteristic peaks of graphite, along with the two sharp diffraction peaks at 2θ angles of ~26°, and a broad peak of 42°~45° (Figure 2a–c). The two sharp peaks of ~26° can be attributed to the turbostratic structure of crystal planes (002) graphite. From Gaussian curve fitting at ~26° using the OriginPro grogram, in H1800 and H2000, turbostratic and graphite constituents were presented. Kasahara et al. and Fogg et al. reported the formation of heterogeneous graphite in thin carbon fibers derived from phenol–formaldehyde resin at high temperature, and three constituents of G-constituent (graphitic), T-constituent (turbostratic) and A-constituent (amorphous) have peaks at ~26.5 and ~26° [28,34]. This implies that the carbon samples are composed of graphite micro-crystallites dispersed and orientated at random across the samples. However, the samples with peaks of carbon allotrope such as carbon tetrahedron (T-carbon), orthorhombic polymorphs (rh6, cR6), a metallic carbon (M-Carbon), (a) H1800 and (b) H2000, showed in graphite contained a week peak centered approximately at 2θ angles of 17.95°, 26.45°, 33.51°, 35.72°, 37.95°, and 38.94° (inset of Figure 2a–c) which perfectly matched with the Figure 2d [35]. In the case of high-temperature carbonization of 1800~2400 without the catalyst, the different XRD phases are visible in graphite: hexagonal (H) and carbon allotrope (CA).

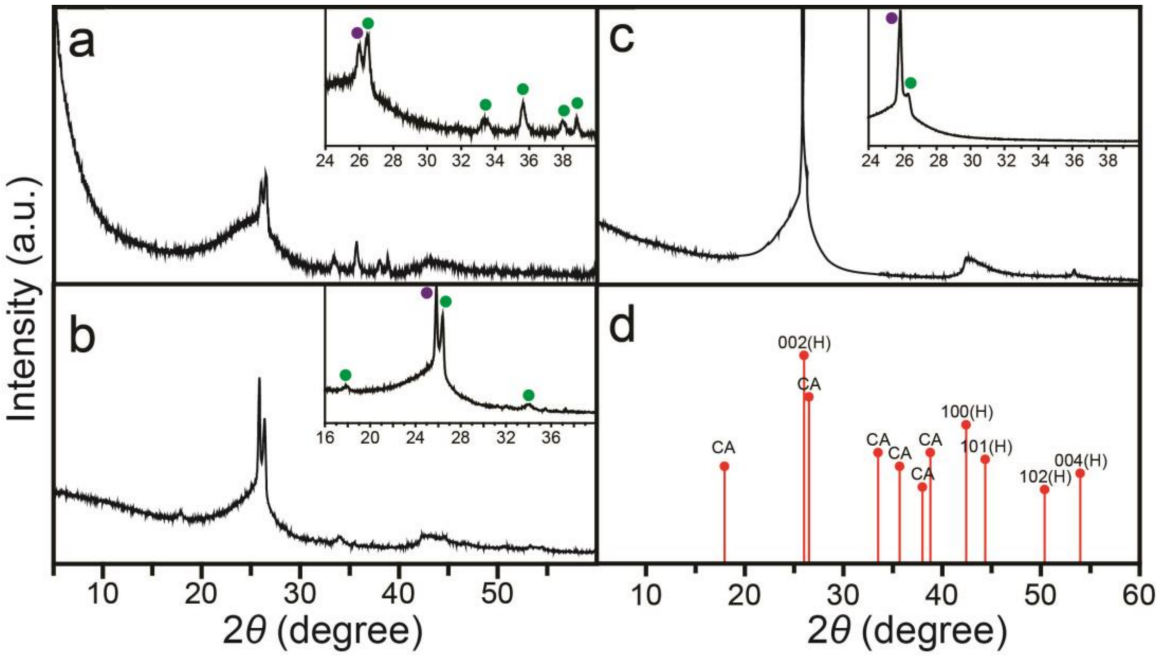

Figure 2. XRD Spectra of graphite for (**a**) H1800, (**b**) H2000, (**c**) H2400, (**d**) graphite of hexagonal (H, •), and carbon allotrope (CA, •) phases such as T, M-carbon, rh6, cR6, and turbostratic constituent.

The diffraction pattern analysis identified the sharp peak at 2θ angles around 26°, enabling the determination of the d_{002} interlayer spacing structural parameter through Gaussian fitting with OriginLab software (version 2023b). Likewise, the broad peaks between 42° and 45° facilitated the calculation of the d_{100} interlayer spacing structural parameter, employing the same approach as for d_{002}. The derived structural parameter values are presented in Table 2. When graphite is heated to 2400 °C, the d_{002} value approximates 0.338 nm, aligning with the lattice spacing of catalyst-synthesized graphite. However, the L_c/d_{002} ratio stands at about 70, which is nearly triple that obtained with a catalyst. Additionally, graphitization degree enhancement is noted up to 2000 °C, beyond which no further increase is observed.

Table 2. Interlayer spacing, crystallite dimension of L_c, L_a, and L_c/d_{002} for H1800, H2000, and H2400.

Samples	d_{002} (nm)	d_{100} (nm)	L_c (nm)	L_a (nm)	L_c/d_{002}
H1800	0.336	0.207	23.931	5.866	71.130
H2000	0.338	0.212	24.555	7.554	72.667
H2400	0.339	0.211	22.997	6.126	67.882

3.2. Functional Group Investigation

FTIR was applied to explore the bonding characteristics and functional groups of C1200, C1000, and commercial graphite, and the representative spectra in a wavenumber range of 4000–800 cm^{-1} are shown in Figure 3. These groups are formed by the oxidation of the carbon atoms on the edges of the graphite layers. The peak at 1740 cm^{-1} is because of the C=O stretching of the carbonyl groups on the surface of graphite. These groups are also formed by the oxidation of the carbon atoms on the edges of the graphite layers [36]. The peak at 1360 cm^{-1} is due to the C-O stretching of the ether groups on the surface of graphite. These groups are formed by the reaction of hydroxyl groups with carbonyl groups. The peak at 1200 cm^{-1} is attributed to the C-H bending of the aromatic rings in the graphite structure. From Figure 4 in C1000, it can also be stated that FTIR spectra display a broad peak around 3350 cm^{-1}, which is due to the stretching mode of the O-H group. The peak at 3350 cm^{-1} corresponds to the O-H stretching of the hydroxyl groups on the surface of graphite [37]. These groups are formed by the reaction of water with the carbon atoms on the edges of the graphite layers when washing with hydrochloric acid.

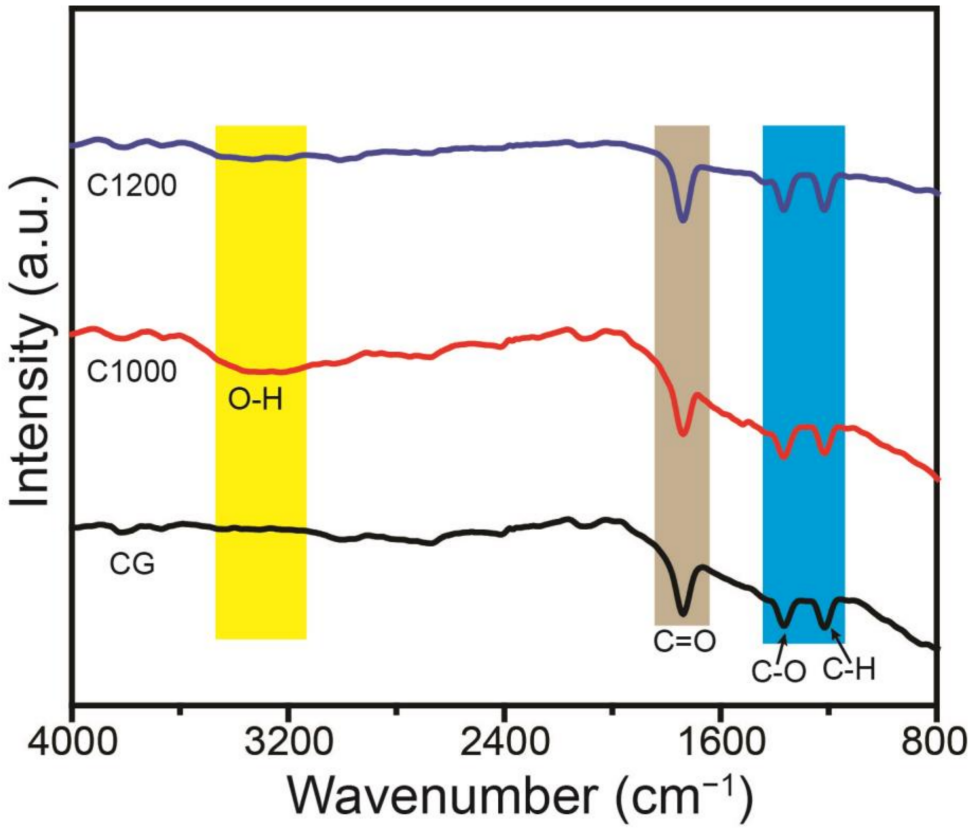

Figure 3. FTIR spectra of C1200, C1000, and CG.

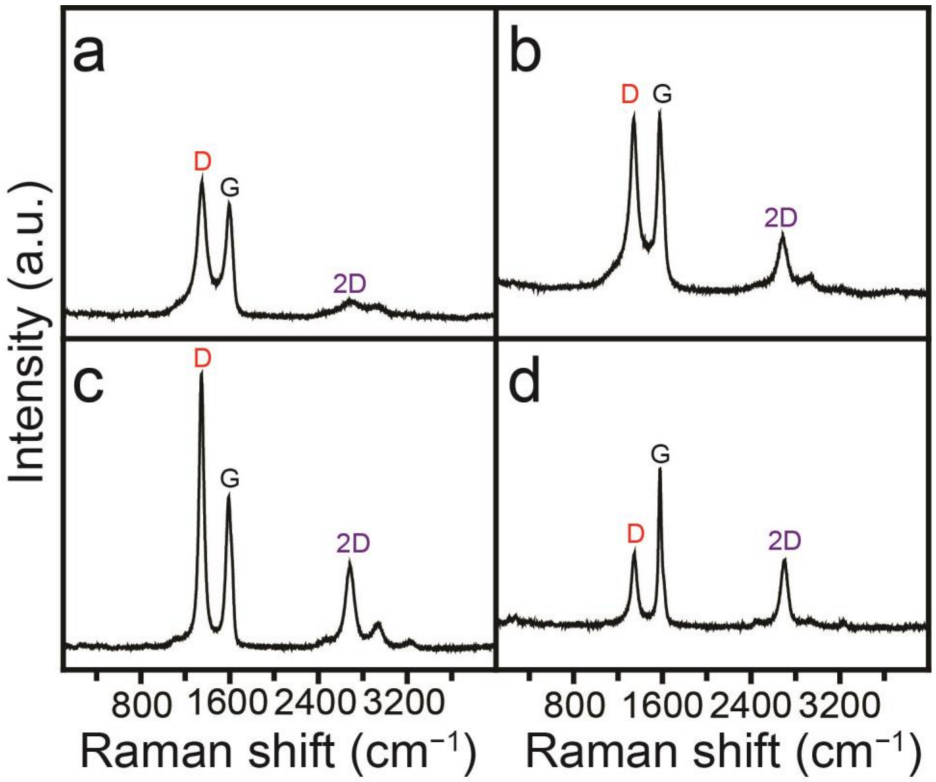

Figure 4. Raman spectra of graphite for (**a**) H1000, (**b**) C1000, (**c**) H1400, and (**d**) C1400.

3.3. Raman Spectra

The Raman spectroscopy results for samples H1000, C1000, H1400, and C1400, as depicted in Figure 4a–d. The presence of the D band peaks around 1345 cm^{-1}, the G band peaks at 1585 cm^{-1}, and the 2D band at 2690 cm^{-1} suggests the transformation of carbon atoms in white charcoal into graphite crystals [38]. The data indicates the formation of disordered graphitic carbon interspersed with graphite crystals. Specifically, the 2D band in H1000, which signifies the presence of graphite crystals, is subdued compared to the other peaks. In contrast, the G band peak in C1400 is more pronounced than its D band peak relative to H1400, indicating a more graphitic layer structure.

The G peak corresponds to the graphitic, or sp^2-bonded carbon atoms, which are arranged in a hexagonal lattice, while the D peak is associated with defects or disorders in the carbon structure, such as sp^3-bonded carbon atoms. A higher intensity (I_G/I_D) ratio indicates a higher degree of graphitization or lower levels of disorder. The integrated intensity ratio of the G peak to the D peak, (I_G/I_D) is useful for measuring the degree of irregularity in carbon materials or the particle size of disordered carbon materials because the D band at 1345 cm^{-1} is related to irregular structure. On the other hand, the equation $I_G/(I_G + I_D)$, as reported by Ramirez-Rico et al. [39] is used to calculate the crystallinity (β) of carbon materials. This ratio normalizes the intensity of the G peak to the total intensity of both G and D peaks, providing a direct measure of the crystalline content relative to the total carbon material. It essentially gives the fraction of the graphitic component in the carbon material. Ramirez-Rico et al. [39] reported that the crystallinity (β) of carbon materials can be obtained using the following Equation (5).

$$\beta = I_G/(I_G + I_D) \quad (5)$$

In Equation (5), I_G and I_D are calculated as the areas under the G (1585 cm^{-1}) and D (1345 cm^{-1}) bands, respectively.

The degree of graphitization, g (%), was calculated using Equation (6) [34].

$$g = (0.3440 - d_{002})/(0.3440 - 0.3354) \quad (6)$$

where 0.3440 is the interlayer spacing in non-graphitized carbon (nm); 0.3354 is the interlayer spacing in an ideal graphite crystallite (nm); and d002 is the interlayer spacing in the sample determined from its XRD pattern (nm).

Table 3 presents the calculated values for the degree of crystallinity (β) and graphitization. C1000 and C1400 exhibited a higher degree of crystallinity than H1000 and H1400, whereas H1000 showed greater crystallinity than H1400; however, the disparity between H1000 and C1000 was marginal. In other words, a comparison between the samples without a catalyst (H1000, H1400) and those with a catalyst (C1000, C1400) at identical temperatures revealed that the catalyst-incorporated samples exhibited elevated values. In the case of degree of graphitization (%), C1000 demonstrated a higher degree of graphitization (%) than C1400. C1000 and H1800 are around 80%, C1400 and H2400 are around 60% of the degree of graphitization. These findings, derived from the d_{002} value, will be discussed further subsequently.

Table 3. Degree of crystallinity (β) and graphitization (%) for all graphite.

Samples	Degree of Crystallinity (β)	Degree of Graphitization (%)
H1000	0.462	-
H1400	0.351	-
C1000	0.498	86.4
C1400	0.678	60.3
H1800 [27]	0.496	87.9
H2400 [27]	0.552	63.0

3.4. Morphological Analysis (FE-SEM and HR-TEM)

Figure 5 shows the surface morphology of the specimens as observed by FE-SEM of C1000 and C1200. In Figure 5a, the particle shape of graphite appears to be a cluster of round particles with small holes. In Figure 5b, the aggregated particles appeared larger. It was verified that, despite differences in cluster size, the round particle sizes were nearly identical in Figure 5c,d, which originated from an enlarged view of the designated region in Figure 5a,b.

The EDS and elemental mapping analysis were employed to ascertain the conformation of elements and the distribution of elements within the C1000 and C1200 samples, as displayed in Figure 6. Figure 6a,b shows that both samples are comprised solely of carbon and oxygen. Specifically, carbon constituted approximately 98.5% of C1000 and 97.7% of C1200, indicating a negligible variance in carbon content of less than 1%. In addition, Figure 6c,d confirms the presentative elements (C and O) distributed homogeneously on the as-synthesized graphite samples. This composition, characterized by the exclusive presence of carbon and oxygen, confirms the absence of extraneous elements in the samples.

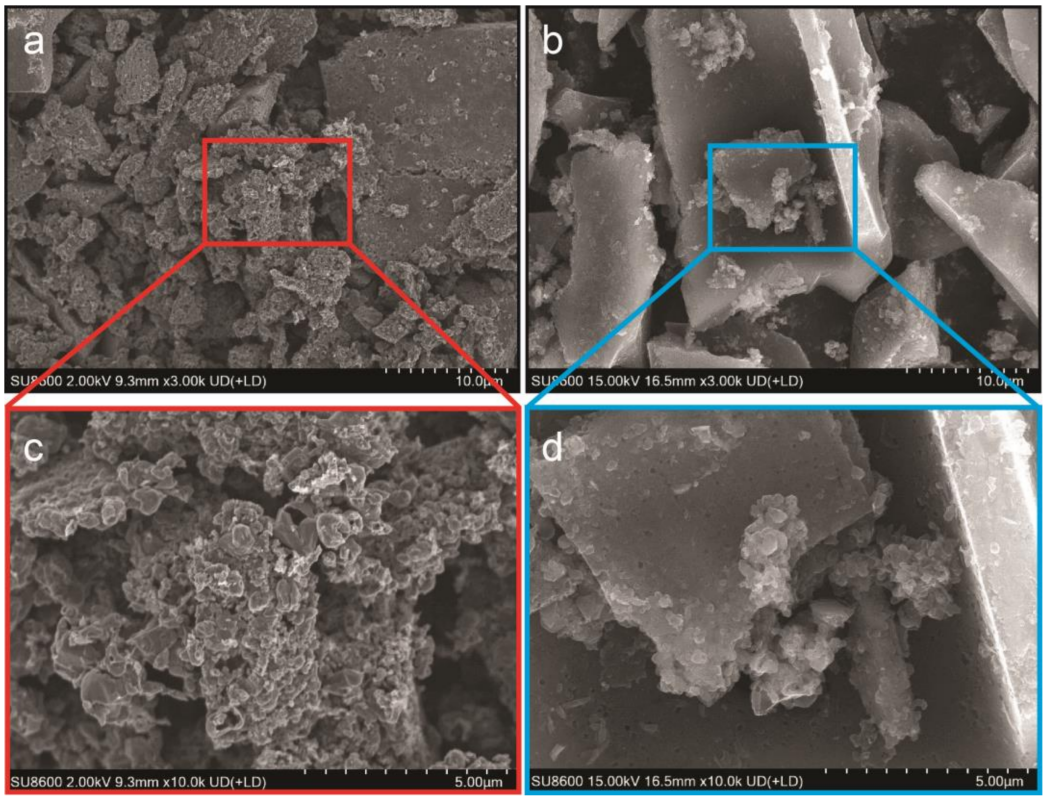

Figure 5. Low and high-resolution FE-SEM images of (**a**,**c**) C1000, and (**b**,**d**) C1200.

The presence of graphene layers and the measured interlayer spacing are important indicators of the degree of graphitization achieved. This provides insight into the material's thermal and electrical conductivity properties as well as its mechanical strength and stability at elevated temperatures. Therefore, HR-TEM images serve as a powerful tool for characterizing microstructural changes and assessing the quality of graphitized materials. Figure 7 shows HR-TEM images detailing the internal structure of the specimens after the graphitization process of white charcoal powder in samples using catalysts of C1000 and C1200. It was confirmed in Figure 7a,b that a graphite layer was formed in all areas within the graphitized sample promoted by the catalyst. These graphite layers are characteristic of the structural transformation that occurs during heat treatment with the catalyst, indicating that the carbon atoms are aligned in a graphite-like structure. A detailed analysis of the HR-TEM images in Figure 7c,d displays the clearly visible graphite layers, signifying the successful conversion of amorphous carbon in white charcoal into a more ordered graphitic form. The average interlayer spacing, the distance between these graphite layers is approximately 0.338 to 0.339 nm. This spacing aligns with the expected measurements for graphitic materials and corroborates with the XRD results, affirming the crystalline nature of the graphite produced. Upon comparison with the results obtained by Park et al. and Fogg et al., it was observed that the lattice spacing of 0.34 nm [26,28] achieved when subjected to high-temperature treatment at 2400 °C and 3000 °C respectively, matched the results obtained using a catalyst at 1200 °C. The interlayer distance of the (002) crystal plane in commercial graphite, as listed in Table 1, was found to be comparable to 0.338 nm. The XRD and TEM analyses confirmed the successful transformation into graphitic material via catalytic (Fe) graphitization at temperatures significantly lower than those required for producing graphite through high-temperature treatment.

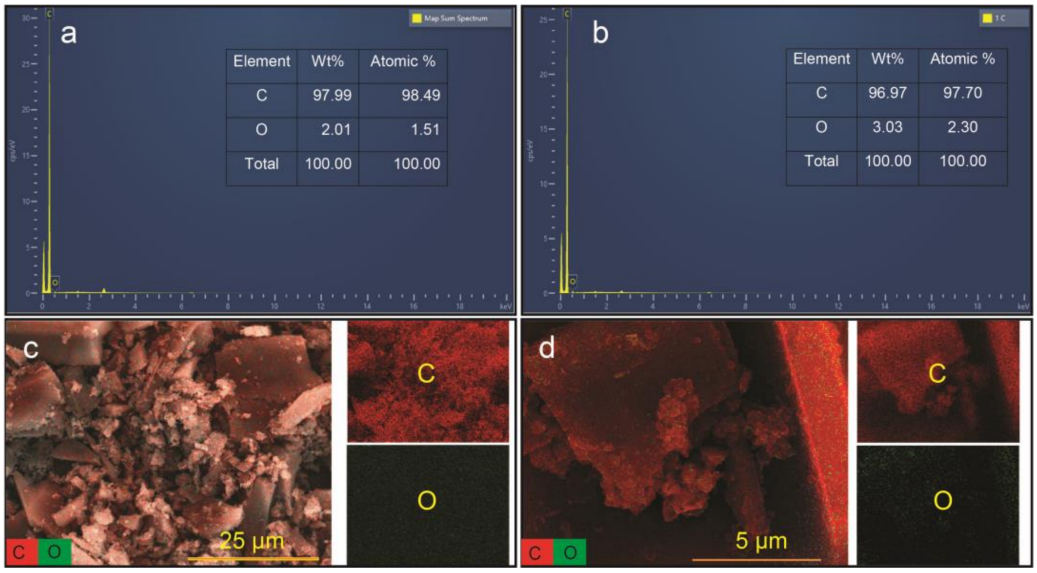

Figure 6. EDS spectra of (**a**) C1000, and (**b**) C1200 and elemental mapping images of (**c**) C1000, and (**d**) C1200 samples.

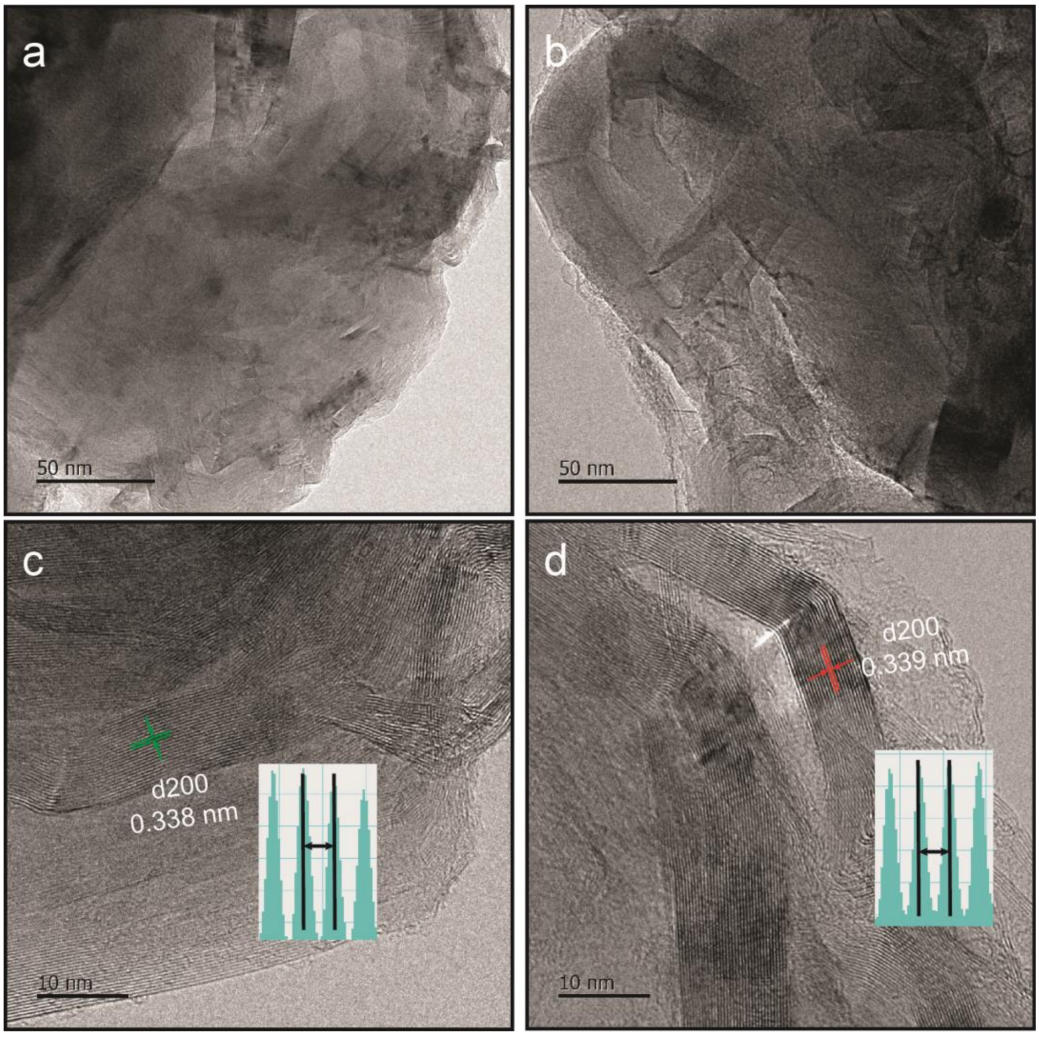

Figure 7. Low and high-resolution HR-TEM images of (**a**,**c**) C1000, and (**b**,**d**) C1200.

4. Conclusions

In this study, we explored the synthesis of graphite from biomass both with and without the use of a catalyst. The catalyst employed was iron nitrate, which allowed for the production of graphite at a significantly lower temperature (reduction by 58.33%) of 1400 °C compared to 2400 °C in the non-catalyzed process. The use of a catalyst resulted in a graphite structure with a d-spacing (d_{002}) of 0.338 nm and a crystallite size (L_c) to d-spacing ratio (L_c/d_{002}) of 29.239 at 1400 °C. In contrast, the absence of a catalyst yielded a larger d-spacing of 0.384 nm and a smaller L_c/d_{002} ratio of 2.330 at the same temperature. At an elevated temperature of 2000 °C, the catalyzed graphite maintained a d-spacing of 0.338 nm and exhibited an increased L_c/d_{002} ratio of 72.667, indicating a higher degree of crystallinity. The X-ray diffraction analysis confirmed that the catalytic process not only lowers the required temperature for graphite formation but also enhances the crystalline quality of the resulting graphite. The investigation into the Degree of Crystallinity (β) and Degree of Graphitization (%) revealed that samples with added catalysts (C1000, C1400) exhibited an increase in these values when compared to their non-catalyst counterparts (H1000, H1400) at equivalent temperatures. The use of a catalyst was further validated by FESEM and EDX analyses, which showed the samples to be composed of over 97 atomic% carbon, free from other impurities. TEM analysis corroborated the successful transformation into graphitic material via catalytic (Fe) graphitization, achieved at significantly lower temperatures than the conventional high-temperature graphite production methods. Therefore, the incorporation of a catalyst is a crucial factor in achieving lower-temperature synthesis of high-quality graphite from wood biomass.

Author Contributions: Conceptualization, S.-K.R., H.S. and Y.S.K.; methodology, M.A.H., S.K., Y.C. and Y.S.K.; software, M.A.H. and Y.S.K.; formal analysis, M.A.H., H.S., Y.C, S.-K.R. and Y.S.K.; investigation, and data curation, M.A.H., H.S., S.K., Y.C. and Y.S.K.; writing—original draft preparation, M.A.H. and Y.S.K.; writing—review and editing, M.A.H. and Y.S.K.; supervision, S.-K.R. and H.G.K.; project administration, H.G.K.; funding acquisition, H.G.K. All authors have read and agreed to the published version of the manuscript.

Funding: The research work described in this article was a part of the basic research project (No. 2016R1A6A1A03012069) supported by the National Research Foundation (Ministry of Education). This work is also supported by the National Research Foundation of Korea (NRF) grant funded by the Korean government (MIST) (No. 2020R1A2C1102174).

Data Availability Statement: The original contributions presented in the study are included in the article, further inquiries can be directed to the corresponding author.

Conflicts of Interest: The authors declare no conflicts of interest.

References

1. Halkos, G.E.; Gkampoura, E.-C. Reviewing Usage, Potentials, and Limitations of Renewable Energy Sources. *Energies* **2020**, *13*, 2906. [CrossRef]
2. Banaś, J.; Utnik-Banaś, K. Using Timber as a Renewable Resource for Energy Production in Sustainable Forest Management. *Energies* **2022**, *15*, 2264. [CrossRef]
3. Surup, G.R.; Trubetskaya, A.; Tangstad, M. Charcoal as an Alternative Reductant in Ferroalloy Production: A Review. *Processes* **2020**, *8*, 1432. [CrossRef]
4. Kalak, T. Potential Use of Industrial Biomass Waste as a Sustainable Energy Source in the Future. *Energies* **2023**, *16*, 1783. [CrossRef]
5. Jara, A.D.; Betemariam, A.; Woldetinsae, G.; Kim, J.Y. Purification, application and current market trend of natural graphite: A review. *Int. J. Min. Sci. Technol.* **2019**, *29*, 671. [CrossRef]
6. Wang, Y.-M.; Zhang, C.-H. Study on Structural Evolution of Synthetic Graphite Derived from Lignite Prepared by High Temperature–High Pressure Method. *Crystals* **2022**, *12*, 464. [CrossRef]
7. Nyathi, M.S.; Clifford, C.B.; Schobert, H.H. Characterization of graphitic materials prepared from different rank Pennsylvania anthracites. *Fuel* **2013**, *114*, 244–250. [CrossRef]
8. Pierson, H.O. Graphite Structure and Properties. In *Handbook of Carbon, Graphite, Diamonds and Fullerenes*; William Andrew Publishing Oxford: Oxford, UK, 1993; pp. 43–69.

9. Wang, X.; Chen, Y.; Yu, C.; Ding, J.; Guo, D.; Deng, C. Preparation and application of ZrC-coated flake graphite for Al_2O_3-C refractories. *J. Alloys Compd.* **2019**, *788*, 739–747. [CrossRef]
10. Alidad, A.; Navik, R.; Gai, Y.; Zhao, Y. Production of pristine graphene quantum dots from graphite by a shear-mixer in supercritical CO_2. *Chem. Phys. Lett.* **2018**, *710*, 64–69. [CrossRef]
11. Wu, Y.; Liu, X.; Xia, D.; Sun, Q.; Yu, D.; Sun, S.; Liu, X.; Teng, Y.; Zhang, W.; Zhao, X. Synthesis of few-layer N-doped graphene from expandable graphite with melamine and its application in supercapacitors. *Chinese Chem. Lett.* **2020**, *31*, 559–564. [CrossRef]
12. Hölscher, F.; Trümper, P.-R.; Junger, I.J.; Schwenzfeier-Hellkamp, E.; Ehrmann, A. Application methods for graphite as catalyzer in dye-sensitized solar cells. *Optik* **2019**, *178*, 1276–1279. [CrossRef]
13. Chung, S.; Shin, D.; Choun, M.; Kim, J.; Yang, S.; Choi, M.; Kim, J.W.; Lee, J. Improved water management of Pt/C cathode modified by graphitized carbon nanofiber in proton exchange membrane fuel cell. *J. Power Sources* **2018**, *399*, 350–356. [CrossRef]
14. Jian, Z.; Piao, Z.Y.; Liu, S.Y.; Su, S.W.; Deng, L.J. Investigation of wear behavior of graphite coating on aluminum piston skirt of automobile engine. *Eng. Fail. Anal.* **2019**, *97*, 408–415. [CrossRef]
15. Dai, T.; Yang, L.; Ning, X.; Zhang, D.; Narayan, R.L.; Li, J.; Shan, Z. A low-cost intermediate temperature Fe/Graphite battery for grid-scale energy storage. *Energy Storage Mater.* **2020**, *25*, 801–810. [CrossRef]
16. Ridgway, P.; Zheng, H.; Bello, A.F.; Song, X.; Xun, S.; Chong, J.; Vincent, B. Comparison of cycling performance of lithium ion cell anode graphites. *J. Electrochem. Soc.* **2012**, *159*, 520–524. [CrossRef]
17. Lee, S.-M.; Kang, D.-S.; Roh, J.-S. Bulk Graphite: Materials and Manufacturing Process. *Carbon Lett.* **2015**, *16*, 135–146. [CrossRef]
18. Mochida, I.; Ohtsubo, R.; Takeshita, K.; Marsh, H. Catalytic graphitization of nongraphitizable carbon by chromium and manganese oxides. *Carbon* **1980**, *18*, 117–123. [CrossRef]
19. Li, S.S.; Wang, J.K.; Zhu, Q.; Zhao, X.W.; Zhang, H.J. Fabrication of Graphitic Carbon Spheres via a Hydrothermal Carbonization Combined Catalytic Graphitization Method Using Cobalt as Catalysts. *Solid State Phenom.* **2018**, *281*, 807–812. [CrossRef]
20. Chen, C.; Sun, K.; Wang, A.; Wang, S.; Jiang, J. Catalytic Graphitization of Cellulose Using Nickel as Catalyst. *BioResources* **2018**, *13*, 3165–3176. [CrossRef]
21. Barnakov, C.N.; Khokhlova, G.P.; Popova, A.N.; Sozinov, S.A.; Ismagilov, Z.R. XRD characterization of the structure of graphites and carbon materials obtained by the low-temperature graphitization of coal tar pitch. *Eurasian Chem. J.* **2015**, *17*, 87–93. [CrossRef]
22. Thompson, E.; Danks, A.E.; Bourgeois, L.; Schnepp, Z. Iron-catalyzed graphitization of biomass. *Green Chem.* **2015**, *17*, 551–556. [CrossRef]
23. Motozuka, S.; Tagaya, M.; Ogawa, N.; Fukui, K.; Nishikawa, M.; Shiba, K.; Uehara, T.; Kobayashi, T. Effective preparation of graphite nanoparticles using mechanochemical solid-state reactions. *Solid State Commun.* **2014**, *190*, 28–32. [CrossRef]
24. Piras, C.C.; Fernández-Prieto, S.; De Borggraeve, W.M. Ball milling: A green technology for the preparation and functionalisation of nanocellulose derivatives. *Nanoscale Adv.* **2019**, *1*, 937–947. [CrossRef]
25. Gómez-Martín, A.; Rutter, M.; Placke, T.; Martínez-Fernández, J.; Ramírez-Rico, J. Iron-catalyzed graphitic carbon materials from biomass resources as anodes for lithium-ion batteries. *Chem. Sus. Chem.* **2018**, *11*, 2776–2787. [CrossRef] [PubMed]
26. Mandal, D.; Vinjamur, M.; Sathiyamoorthy, D. Hydrodynamics of beds of small particles in the voids of coarse particles. *Powder Technol.* **2013**, *235*, 256–262. [CrossRef]
27. Park, Y.-N.; Lee, J.J.; Kwac, L.-K.; Ryu, S.-K.; Kim, H.-G. Graphitization of Oak tree-based White Charcoals by High Temperature Heat Treatment. *Korean J. Chem. Eng.* **2024**, *41*. [CrossRef]
28. Fogg, J.L.; Putman, K.J.; Zhang, T.; Lei, Y.; Terrones, M.; Harris, P.J.F.; Marks, N.A.; Suarez-Martinez, I. Catalysis-free transformation of non-graphitising carbons into highly crystalline graphite. *Commun. Mater.* **2020**, *1*, 47. [CrossRef]
29. Nakayasu, Y.; Goto, Y.; Katsuyama, Y.; Itoh, T.; Watanabe, M. Highly crystalline graphite-like carbon from wood via low-temperature catalytic graphitization. *Carbon Trends* **2022**, *8*, 100190. [CrossRef]
30. Hanif, M.A.; Kim, Y.S.; Ameen, S.; Kim, H.G.; Kwac, L.K. Boosting the Visible Light Photocatalytic Activity of ZnO through the Incorporation of N-Doped for Wastewater Treatment. *Coatings* **2022**, *12*, 579. [CrossRef]
31. Zheng, H.; Xu, R.; Zhang, J.; Daghagheleh, O.; Schenk, J.; Li, C.; Wang, W. A Comprehensive Review of Characterization Methods for Metallurgical Coke Structures. *Materials* **2021**, *15*, 174. [CrossRef]
32. Li, S.K.; Zhu, Y.M.; Wang, Y.; Liu, J. The Chemical and Alignment Structural Properties of Coal: Insights from Raman, Solid-State (13)C NMR, XRD, and HRTEM Techniques. *ACS Omega* **2021**, *6*, 11266–11279. [CrossRef] [PubMed]
33. Deraman, M.; Sazali, N.E.S.; Hanappi, M.F.Y.M.; Tajuddin, N.S.M.; Hamdan, E.; Suleman, M.; Othman, M.A.R.; Omar, R.; Hashim, M.A.; Basri, N.H.; et al. Graphene/semicrystalline-carbon derived from amylose films for supercapacitor application. *J. Phys. Conf. Ser.* **2016**, *739*, 12085. [CrossRef]
34. Destyorini, F.; Irmawati, Y.; Hardiansyah, A.; Widodo, H.; Yahya, I.N.D.; Indayaningsih, N.; Yudianti, R.; Hsu, Y.-I.; Uyama, H. Formation of nanostructured graphitic carbon from coconut waste via low-temperature catalytic graphitisation. *Eng. Sci. Technol. Int. J.* **2021**, *24*, 514–523. [CrossRef]
35. Zhao, C.-X.; Niu, C.-Y.; Qin, Z.-J.; Ren, X.; Wang, J.-T.; Cho, J.-H.; Jia, Y. H_{18} carbon: A new metallic phase with sp^2-sp^3 hybridized bonding network. *Sci. Rep.* **2016**, *6*, 21879. [CrossRef]
36. Koçanalı, A.; Apaydın Varol, E. An Experimental Study on the Electrical and Thermal Performance of Reduced Graphene Oxide Coated Cotton Fabric. *Int. J. Energy Res.* **2021**, *45*, 12915–12927. [CrossRef]
37. Hanif, M.A.; Shin, H.; Chun, D.; Kim, H.G.; Kwac, L.K.; Han, S.-W.; Kang, S.-S.; Kim, Y.S. Development of Highly Ultraviolet-Protective Polypropylene/TiO_2 Nonwoven Fiber. *J. Compos. Sci.* **2024**, *8*, 86. [CrossRef]

38. Sadezky, A.; Muckenhuber, H.; Grothe, H.; Niessner, R.; Poschl, U. Raman micro spectroscopy of soot and related carbonaceous materials: Spectral analysis and structural information. *Carbon* **2005**, *43*, 1731–1742. [CrossRef]
39. Ramirez-Rico, J.; Gutierrez-Pardo, A.; Martinez-Fernandez, J.; Popov, V.V.; Orlova, T.S. Thermal conductivity of Fe graphitized wood derived carbon. *Mater. Des.* **2016**, *99*, 528–534. [CrossRef]